Optics Letters

Coherent beam combining of optical vortices

Hossein Fathi,[1,*] Mikko Närhi,[1] Rafael Barros,[1,2] and Regina Gumenyuk[1,3]

[1]Laboratory of Photonics, Physics Unit, Faculty of Engineering and Natural Sciences, Tampere University, 33720 Tampere, Finland
[2]Instituto de Física, Universidade de São Paulo, 05315-970 São Paulo, SP, Brazil
[3]Tampere Institute for Advanced Study, Tampere University, Kalevantie 4, Tampere 33100, Finland
*hossein.fathi@tuni.fi

Received 28 February 2024; revised 29 May 2024; accepted 30 May 2024; posted 3 June 2024; published 5 July 2024

We experimentally demonstrate the power scaling of optical vortices using the coherent beam combining technique, encompassing topological charges ranging from $\ell = 1$ to $\ell = 5$ realized on the basis of a Yb-doped fiber short-pulsed laser system. The combining efficiency varies from 83.2 to 96.9% depending on the topological charge and beam pattern quality generated by the spatial light modulators. This work is a proof of concept for using a coherent beam combining technique to surpass the physical power/energy limitation of any single source of optical vortices, regardless of the generation methods employed. These results open a pathway to power scaling of optical vortices with diverse applications in science and industry by utilizing advances in light–matter interactions.

https://doi.org/10.1364/OL.522633

Optical vortices (OVs), spiral-shaped light beams with orbital angular momentum (OAM), have undergone substantial advancements and gained extensive interest since their introduction in 1989 [1–3]. By precisely tailoring the spatial structure of the beam, researchers can manipulate their properties and achieve functionalities beyond those of traditional Gaussian beams. OVs are characterized by transverse phase patterns of the form $\exp(i\ell\varphi)$, where ℓ is an integer called the topological charge (TC), and φ is the azimuthal angle. Due to their spiral wavefronts, OVs carry OAM equivalent to $\ell\hbar$ per photon, which is ℓ times larger than the spin angular momentum (SAM), which is $\pm\hbar$ per photon. These unique properties make them highly promising in a variety of applications, such as optical tweezers, high-capacity optical communications, super-resolution microscopy, and laser–plasma interaction [3]. Furthermore, improving the tunability of OVs, encompassing their spectral and temporal characteristics spurred progress in various fields of advanced research [3].

Two primary techniques for generating OVs involve direct generation within the laser cavity and indirect mode conversion via phase front modulators such as spatial light modulators (SLMs) acting as computer-generated holograms, spiral phase plates, q-plates, and cylindrical lenses [4].

There has been a sustained interest in generating high-power spatially structured beams to fully exploit their potential applications, such as mitigating attenuation challenges in free-space optical communication, enabling robust optical trapping and manipulation, and facilitating high-power laser material processing [3–6]. However, generating high-power OVs using conventional methods encounters limitations due to the thermal damage to components. To address this issue, we demonstrate the capability of coherent beam combining (CBC) as a versatile technique for power scaling OVs. In particular, we present experimentally the first-ever direct combination of two OV beams with multiplication of the average power realized in a filled-aperture configuration. In contrast, earlier reports have combined Gaussian beams to create OVs at a fixed position by utilizing a tiled-aperture configuration [7–12].

CBC in the filled-aperture configuration is a method to increase the power output of lasers by combining multiple laser amplifiers initially seeded by a common source, preserving the spatial properties of the output beam [13,14]. The main idea involves splitting a seed laser into multiple replicas (N channels), amplifying each replica to its maximum power/energy through separate amplifier sections, and subsequently combining them into a single high-intensity beam while preserving the beam's quality. Along with preserving the spatial properties, CBC in the filled aperture configuration also ensures the retention of the spectral properties of the laser. This technique relies on establishing a fixed phase relationship between the laser amplifiers, enabling them to operate effectively as a single laser amplifier. To date, experimental demonstrations have shown average powers exceeding 100 kW, pulse energies reaching a few tens of millijoules, and peak powers reaching a few tens of gigawatts [13–17]. Furthermore, CBC reveals significant potential for scaling the number of channels, as experimental demonstrations have shown CBC of 107 beams [18].

In this paper, we employ the CBC technique in the filled aperture configuration for power scaling of OVs. This method is a generic tool for power/energy scaling and can be utilized with any of the various techniques for generating OVs. In our experiment, we use spatial light modulators (SLMs) to generate linearly polarized OVs with topological charges spanning from $\ell = 1$ to $\ell = 5$. The SLMs provide flexibility in the generation of different OVs by changing the computationally applied pattern only, therefore minimize the alignment routine in the setup when changing from one OV type to another. The beam combining efficiency depends on the OV beam quality and spatial

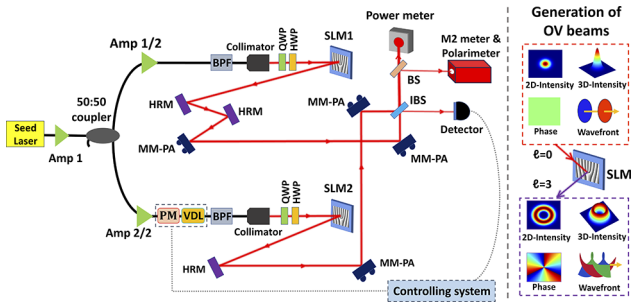

Fig. 1. Scheme of the experimental setup for the generation and coherent combination of optical vortices. The schematic process of the generation of the $\ell = 3$ OVs out of Gaussian beams is shown on the right side of the picture. The components are labeled as follows: Amp, amplifier; PM, phase modulator; VDL, variable delay line, BPF, bandpass filter; QWP, quarter wave plate; HWP, half-wave plate; SLM, spatial light modulator; HRM, high reflective mirror; MM-PA, motorized mirror equipped with piezo actuators; IBS, intensity beam splitter; BS, beam sampler.

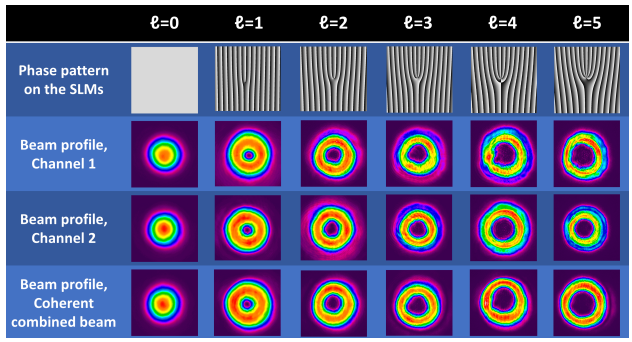

Fig. 2. Profiles of five distinct linearly polarized Laguerre–Gaussian optical vortices, OVs ($\ell = 1$–5), and a Gaussian beam, for two different channels and their coherent combination along with the corresponding fork phase patterns applied on SLM.

pattern complexity of the generated vortices and can be as high as ~96.9%, roughly analogous to the combining efficiency for Gaussian beams.

Figure 1 illustrates the experimental setup employed for the generation and coherent combination of OVs. The scheme highlights the key components and techniques utilized in generating and combining OVs. The seed source consists of a gain-switched laser that emits pulses at a repetition rate of 20 MHz, with a pulse duration of 55 ps (±5ps). Following the amplification in the initial stage, the seed laser is split into two channels using a 50:50 fiber coupler. Subsequently, each channel undergoes a second amplification stage, delivering an average power of up to 100 mW. The second channel is equipped with a LiNbO3 electro-optic phase modulator (PM) to precisely adjust the relative phase of the OVs to achieve a coherent combination. As we operate with pulsed sources, a variable delay line (VDL) is incorporated to equalize the optical path lengths of the CBC channels. Both channels incorporate a fiber in-line optical bandpass filter (BPF) with a bandwidth of ±2 nm at 1040 nm to suppress the spontaneous emission generated in preamplifier stages. Two collimators are employed at the end of each channel to collimate the output beams for propagation in free space. SLMs with fork phase patterns are used to generate approximate Laguerre–Gaussian (LG) optical vortex beams with different TCs ($\ell = 1$–5). Alternatively, other methods can be employed for the generation, such as utilizing Q-plates and volume Bragg gratings (VBGs). For illustrative purposes, the schematic process for generating OVs with $\ell = 3$ from an input Gaussian field is depicted on the right side of Fig. 1. Due to the polarization dependency of the SLMs, we employ a pair of a quarter-wave plate (QWP) and a half-wave plate (HWP) to achieve the optimal polarization state. Subsequently, each generated OV is directed toward a set of high reflection mirrors (HRMs) that steer the beams into the combining elements. To ensure precise spatial overlapping and maximize the combining efficiency, each channel utilized two high-reflection motorized mirrors equipped with piezo actuators. These actuators enable fine adjustments of the mirror positions, ensuring accurate alignment of the OVs. The setup is built in a filled-aperture configuration, employing near-field beam combining. The combining element is an intensity beam splitter (IBS), facilitating the spatial overlap and coherent combination of the two OVs. IBSs are preferred due to their lower coating absorption compared to polarizer beam splitters (PBS) and their lower cost compared to diffractive optical elements (DOEs), making them a more suitable choice for this work [10,11]. The coherently combined beam emerges from a predetermined port of the intensity beam splitter. Using a beam sampler (BS), a portion of the combined beam is extracted to measure the beam quality factor. The uncombined light that emerges from the idler port of the IBS is utilized as feedback for the active control system. The beam phase control system is based on the single-detector electronic frequency-tagging algorithm (LOCSET) controlled by a commercial feedback loop system (Laselock, TEM Messetechnik) [19].

Experimentally measured combining efficiency is typically defined as the ratio of the power/energy in the combined beam to the sum of the power/energies of the beams before combining [20]. For the five studied OVs, combining efficiencies of 96.9% ($\ell = 1$), 93.2% ($\ell = 2$), 90.3% ($\ell = 3$), 85.6% ($\ell = 4$), and 83.2% ($\ell = 5$) were achieved. As a reference measurement, two Gaussian beams were coherently combined with an efficiency of 98.3%. Figure 2 illustrates the beam profiles of the five measured OVs and a Gaussian beam for two different channels, along with their coherent combination output. Additionally, it shows the corresponding fork phase patterns applied on SLM to generate OVs from the input Gaussian fields. The supplementary videos (Visualization 1, Visualization 2, and Visualization 3) depict the time-varying beam profiles of the combined OV beams with $\ell = 0$, 1, and 5 when the phase control system is on (coherently combination) and off (random combination). Other OVs ($\ell = 2$–4) demonstrated similar behavior during combination.

The experimental results reveal that the CBC efficiencies of OVs drop from 96.9% to 83.2% by increasing the TC from 1 to 5. We obtain a high combining efficiency for the fundamental mode, only limited by technical imperfections in the experimental setup, such as imperfect alignment and aberrations imprinted by the SLM screens upon reflection. For the higher-order modes, we observe a decrease in combining efficiency with increasing topological charge. The main reason behind this effect is that we generate the OVs by simply applying a spiral phase $\exp(i\ell\varphi)$ to a Gaussian beam; the obtained fields are not pure Laguerre–Gaussian modes LG (ℓ,0), but rather superpositions of modes LG (ℓ, p) of different radial orders. This distinction is

important because the Gouy phase delay experienced by higher-order modes amounts to $\phi_G = (2p + |\ell| + 1)\tan^{-1}(z/z_R)$, where z_R is the Rayleigh range, which increases with the radial order p. Consequently, the optimal coherent combination of superpositions of LG (ℓ, p) requires the free-space propagation lengths of the two beam paths between the SLMs and the IBS to be identical. This was not the case of our experiment where a free-space length difference of ~30 cm was necessary to compensate for mismatched optical paths in the fiber components. To show that this is the reason for the decrease in combining efficiency in our experiment, we simulated the CBC of OVs with our experimental parameters, see Supplement 1, Figs. S1 and S2. The simulation results show excellent agreement with the experimental results, showing that the CBC of OVs with matched free-space lengths should be nearly as efficient as for Gaussian fields.

We emphasize that the imperfect combining efficiency is not a fundamental limitation of OAM modes. The near-perfect combining efficiency could be achieved by preparing pure Laguerre–Gaussian modes on the SLM, in which case the Gouy phase difference of the single mode could be compensated by the phase-locking mechanism. However, the preparation of pure LG modes requires either amplitude modulation [21] or more complex techniques such as a multi-plane light conversion [22]. Although the latter can be lossless in principle, the current state-of-the-art still requires multiple reflection on an SLM screen, thereby introducing undesirable losses in the mode preparation. Unraveling all the contributing factors affecting the combining efficiency of OVs requires in-depth theoretical and experimental investigations which lie beyond the scope of this contribution. However, this matter has primarily been explored in the context of CBC of Gaussian beams, where the impact of various key parameters on the combining process has been discussed in detail [23,24].

Supplement 1, Fig. S3 provides an example of how improvement in the quality of the generated OVs can increase their combining efficiencies. We conducted two similar experiments of generation and combination of OVs, differing only in the phase patterns used for the generation of OVs. We demonstrated that changing the phase patterns from spiral to fork on the SLMs resulted in more symmetric beam profiles for OVs, consequently leading to higher combining efficiency. By changing the phase pattern from spiral to fork, the combining efficiencies of OVs with $\ell = 1, 2, 3, 4$, and 5 increased from 95.5%, 86.9%, 83.2%, 78%, and 68.1% to 96.9%, 93.2%, 90.3%, 85.6%, and 83.2%, respectively. The lower CBC efficiency with the spiral holograms is caused by contamination from a Gaussian component that is not modulated by the SLM, which is not optimally combined due to the aforementioned Gouy phase problem. Figure 2 only shows the result with the fork pattern.

The output beam qualities of all combined OVs were analyzed based on the ISO 11146-compliant M^2 factor measurement for Gaussian beams, which defines how tightly a laser beam can be focused under certain conditions (see Fig. 3). However, there is no single standardized parameter (like the beam quality factor for Gaussian beams) for quantifying OVs. The quality of OVs is often described by several parameters, such as intensity distribution profile, and mode purity. We would like to note that the combined beam demonstrated higher uniformity of intensity distribution. This can be interpreted as an improvement of the beam quality by CBC, attributable to the coherent filtering effect [Ref. 13, sec 2]. Due to this effect, only the coherent parts of the beam that have the same properties (polarization, phase, wavefront) will be coherently combined, and the rest of the beam will not combine and get out in the loss channel. Figure 3(a) depicts the measurement of the beam quality factor of the combined beams for six different orders of OVs, along with their corresponding combining efficiencies. Figure 3(b), illustrates the M^2-curve of the coherently combined beams for OVs with $\ell = 0$, 1, and 5,accompanied by the corresponding near-field beam profiles as insets. We present three of six beams as examples, and other OVs demonstrated similar performance. The depicted beam quality factors and beam widths in Fig. 3 clearly indicate that as the topological charge increases, there is a corresponding beam asymmetry, thereby signifying a degradation in quality for high-order OVs.

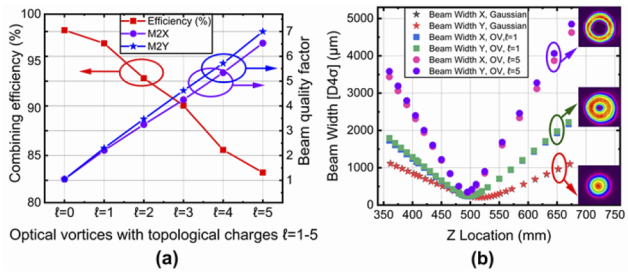

Fig. 3. Analysis of the beam quality and combining efficiency of the combined beams. (a) ISO 11146-compliant M^2-measurement of the combined beams with the 4σ-method with corresponding combining efficiencies, (b) M^2-curve of the combined beams of OVs with $\ell = 0$, 1, and 5 (Insets: near-field beam profiles of the combined beams.)

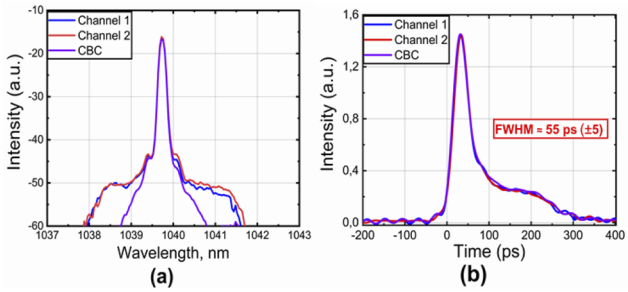

Fig. 4. Optical spectrum and pulse duration measurements of the output of channel 1, channel 2, and the combined output of both channels for an OV with $\ell = 1$. (a) Normalized optical spectra and (b) time-domain envelope measured using a 25-GHz photodetector.

The typical optical spectrum of both channels and the combined one for $\ell = 1$ are depicted in Fig. 4(a). The width of the amplified spontaneous emission (ASE) in the spectra of the individual beams, the pedestal region, is attributed to the utilization of BPFs in the fiber part of the experimental setup. However, the spectrum of the combined beam exhibits a narrower width of ASE owing also to the coherent filtering effect [Ref. 13, sec 2]. Indeed, the shoulders of the individual beams which are caused by ASE from the amplifiers are incoherent in polarization and phase by nature, thereby are not combined. For further analysis, we characterized the optical pulse durations of both individual channels and the combined output in the time domain using a 25-GHz photodetector, as illustrated in Fig. 4(b). We have not noticed any spectral or temporal profile changes for other OVs. Polarization and

output power stability assessment was conducted on the combined $\ell = 1$ beam over 20 min using a commercial polarimeter (PAX1000IR2/M), providing a clear illustration of the excellent polarization and power stability of the CBC system, see Supplement 1, Fig. S4. The standard deviation of the output power was 1.1%, while DOP variations did not exceed 0.2%.

In conclusion, we have presented the first experimental demonstration of coherent beam combining for optical vortices, to the best of our knowledge. In this proof-of-concept work, the number of channels was limited to two, and power levels were limited to 100 mW level due to the SLM power handling capability. However, technically upscaling the number of channels or using other means for OV generation can easily supersede the power levels reported in the manuscript. We observed a drop in combining efficiencies as the topological charge increased from 1 to 5. We identify two primary reasons for this: beam quality and associated with it is a Gouy phase effect, as there was a difference in free-space optical length for different channels. As higher-order modes were filtered due to the discrepancy of accumulated phases at the combining point, the combined beam demonstrated improved uniformity of the spatial intensity distribution for all OVs, which could be interpreted as improved beam quality. To maximize the combining efficiency, one needs either to generate the pure beam or to equalize the free-space parts in the channels. However, in the latter case, the beam quality of the combined beam is unlikely to be improved. We envision that the results can benefit the power/energy scaling of optical vortices in short-pulsed laser systems, thereby paving the way for exploring novel applications in the field of high-intensity light–matter interactions or overcoming signal attenuation in long-distance free-space optical communications utilizing OAM beams.

Funding. Research Council of Finland (349120, 320165); Horizon Europe EIC Pathfinder-OPEN (101096317).

Acknowledgment. The authors thank Robert Fickler, Hassan Asgharzadeh, and Ebrahim Aghayari for fruitful discussions.

Disclosures. The authors declare no conflicts of interest.

Data availability. Data underlying the results presented in this paper are not publicly available at this time but may be obtained from the authors upon reasonable request.

Supplemental document. See Supplement 1 for supporting content.

REFERENCES

1. P. Coullet, L. Gil, and F. Rocca, Opt. Commun. **73**, 403 (1989).
2. L. Allen, M. Beijersbergen, R. Spreeuw, *et al.*, Phys. Rev. A **45**, 8185 (1992).
3. Y. Shen, X. Wang, Z. Xie, *et al.*, Light: Sci. Appl. **8**, 90 (2019).
4. X. Wang, Z. Nie, Y. Liang, *et al.*, Nanophotonics **7**, 1533 (2018).
5. G. Xie, L. Li, Y. Ren, *et al.*, Optica **2**, 357 (2015).
6. A. Goffin, I. Larkin, A. Tartaro, *et al.*, Phys. Rev. X **13**, 011006 (2023).
7. L. Wang, L. Wang, and S. Zhu, Opt. Commun. **282**, 1088 (2009).
8. T. Hou, D. Zhi, R. Tao, *et al.*, Opt. Express **26**, 14945 (2018).
9. D. Zhi, T. Hou, P. Ma, *et al.*, High Power Laser Sci. Eng. **7**, E33 (2019).
10. M. Veinhard, S. Bellanger, L. Daniault, *et al.*, Opt. Lett. **46**, 25 (2021).
11. J. Long, T. Hou, Q. Chang, *et al.*, Opt. Lett. **46**, 3665 (2021).
12. J. Long, K. Jin, Q. Chen, *et al.*, Opt. Lett. **48**, 5021 (2023).
13. A. Brignon, ed., *Coherent Laser Beam Combining* (John Wiley & Sons, 2013).
14. H. Fathi, M. Närhi, and R. Gumenyuk, Photonics **8**, 566 (2021).
15. S. J. McNaught, C. P. Asman, H. Injeyan, *et al.*, Front. Opt. **1**, FThD2 (2009).
16. M. Müller, C. Aleshire, A. Klenke, *et al.*, Opt. Lett. **45**, 3083 (2020).
17. H. Stark, J. Buldt, M. Müller, *et al.*, Opt. Lett. **44**, 5529 (2019).
18. H. Chang, Q. Chang, J. Xi, *et al.*, Photonics Res. **8**, 1943 (2020).
19. T. M. Shay, V. Benham, J. T. Baker, *et al.*, IEEE J. Sel. Top. Quantum Electron. **13**, 480 (2007).
20. V. E. Leshchenko, Opt. Express **23**, 15944 (2015).
21. E. Bolduc, N. Bent, E. Santamato, *et al.*, Opt. Lett. **38**, 3546 (2013).
22. N. K. Fontaine, R. Ryf, H. Chen, *et al.*, Nat. Commun. **10**, 1865 (2019).
23. A. Klenke, E. Seise, J. Limpert, *et al.*, Opt. Express **19**, 25379 (2011).
24. G. D. Goodno, C. C. Shih, and J. E. Rothenberg, Opt. Express **20**, 23587 (2012).